Chapter-4 Reduced Graphite Oxide and MoS_2 Based Electrodes for Supercapacitors

4.1 Introduction

The imminent exhaustion of fossil fuels, their soaring price and the associated alarming global warming situation have triggered the urge to develop a sustainable and renewable energy source. Renewable energy sources (solar, wind and hydroelectric) are regarded as next-generation energy sources, but the sun does not shine at all times, and the wind does not always blow. So, due to their intermittent nature, imbalanced regional distribution and low energy density, these energy sources do not show potential impact unless they are integrated with efficient energy storage technologies [83], [190]. To resolve issues related to energy demand, the research community needs to design clean, efficacious, economical, and eco-friendly energy storage and conversion systems. For these reasons, devices like capacitors, conventional batteries, fuel cells, and supercapacitors are contemplated as electrical and electrochemical storage systems [191,192]. These devices can be used in the transportation industry, as well as in consumable and industrial electronic devices. The different structural/ assembly and charge-discharge capacities of conventional capacitors, supercapacitors, and batteries are displayed in **Figure 4.1**. The efficiency of various energy conversion and storage devices are determined by their energy and power densities [193,194] . The conventional capacitors store the energy via coulombic interaction of opposite electrodes, while redox reaction at electrodes is responsible for energy storage in battery. Hence, capacitors are expected to deliver high power and batteries are expected to deliver high energy, while supercapacitors are aimed to bridge the gap between them, as shown in the Ragone plot of **Figure 4.2** [91].

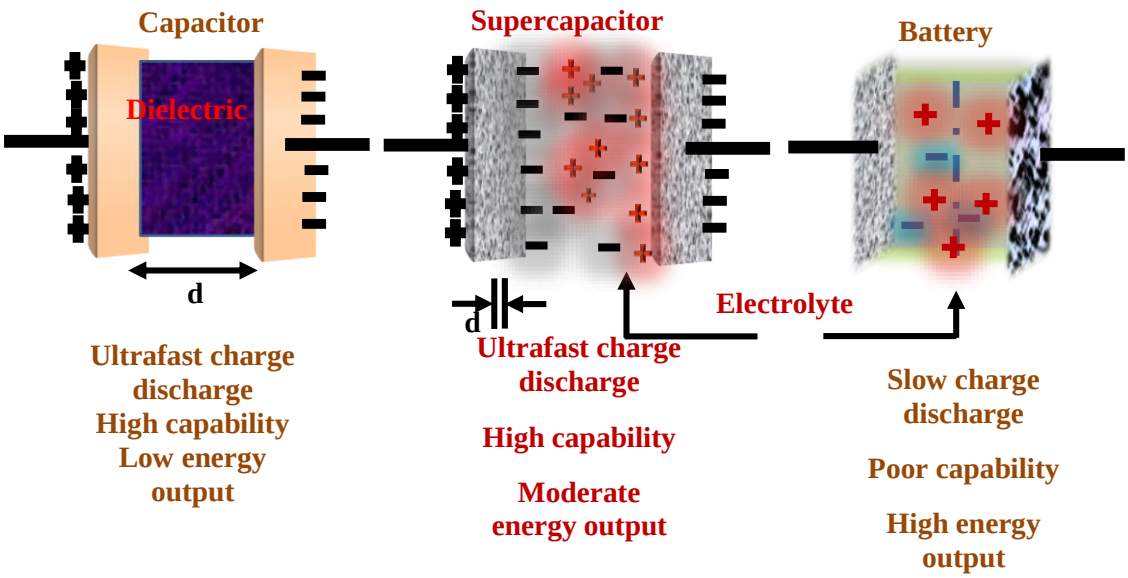

Figure 4.1 *Configurational outlines of conventional capacitors, supercapacitors and batteries.*

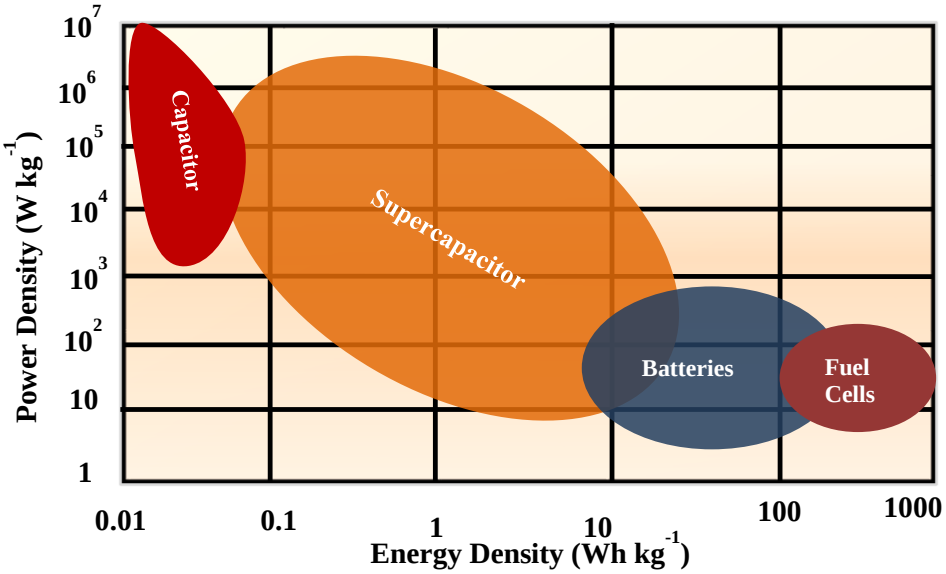

Figure 4.2 *Ragone plot for different energy storage and conversion devices.*

The conventional capacitors deliver high power density (10^6 W kg^{-1}) and can provide higher current than batteries, but their energy density (0.1 Wh kg^{-1}) is limited. So, they do not store enough energy to work as energy storage by themselves [195,196]. Batteries like Li-ion, Li-air, Na- ion etc. are regarded as energy sources (~ 406 Wh kg^{-1}), but they suffer with a long charging time and slow power delivery < 250 W kg^{-1}. The extensive use of batteries

is usually done in energy storage systems where low power and high energy is required. A device with both high energy and high-power density would be ideal in the energy storage domain. To store the electrochemical energy, supercapacitors (SCs) are known as viable energy-storage devices owing to their high cyclic durability and power density. Due to the high-power density, SCs hold great promise as energy storage devices in high-power hybrid vehicles. However, the energy density of SCs is still insufficient, which prevents the large-scale utilization of supercapacitors. As a result, the production of efficient and cost-effective electrode material for SCs showing long-term durability, high capacitance and energy density remains a significant issue. Carbon nanostructures (Activated carbon, nanotubes and graphene or reduced graphite oxides) having a high surface area, mesoporosity and good electrical conductivity are known to be suitable for supercapacitor electrodes [197–199]. Additionally, carbon-based nanocomposites with transition metal oxides (RuO_2, MnO_2 etc) and conducting polymers (polyaniline, polypyrrole etc.) have been investigated to achieve higher pseudo-capacitance [82], [200–202]. Still, they suffer from poor cycle stability due to structural degradation of electrodes during redox processes. Therefore, a significant focus has been on improving the capacitance of pristine carbon nanostructures such as carbon nanotubes, graphene, and reduced graphite oxides (rGO) which are stable during the electrochemical process. As rGO is a cost-effective electrode in comparison to other carbon nanostructures, various thermo-chemical exfoliation processes have been explored for rGO synthesis using different reducing agents and temperature/pressure conditions. The low-temperature exfoliation process is preferred due to less energy consumption and greater control over the homogeneity of the sample. Different reducing agents such as hydrogen iodide [203], hydrochloric acid [204], ethylene glycol [205], hydrazine hydrate [107], urea [206], formic acid [207], sodium borohydride [208] etc. have been evaluated for low temperature reduction of graphite oxide (GO) in the

temperature range 100 to 200 °C. Stoller *et al.* [107] demonstrated a specific capacitance of 135 F g^{-1} at a current density around 1 A g^{-1} with 5.5 M KOH electrolyte for rGO prepared at 100 °C for 24 h using hydrazine hydrate. Lai *et al.* [206] showed a specific capacitance of 255 F g^{-1} at a low current density of 0.5 A g^{-1} in 6M KOH for rGO prepared at 90 °C for 12 h using urea. Rajagopalan *et al.* [209] showed specific capacitance of 253 F g^{-1} at 0.2 A g^{-1} current density with 2M H_2SO_4 electrolyte for KOH treated rGO, reduced with hydrazine hydrate at 95 °C for 24 h. Different performances of rGO based supercapacitors are attributed to the quality of the sample which includes its wettability, surface area and electrical conductivity [210].

In addition to carbon nanostructures, transition metal dichalcogenides (TMDCs) nanostructures are also known as a new class of promising candidates for energy generation and storage in last few years. Among TMDCs, MoS_2 attracted considerable attention as an electrode for supercapacitor application due to its low cost, earth abundance and chemical stability. The electrochemical performance of bulk MoS_2 is hindered by its low intrinsic conductivity and ease of aggregation. The significant exposure of edge sites of unsaturated sulphur atoms of MoS_2 compared to its basal plane leads to maximum electrochemical activity [137]. The centre molybdenum atom of the lamellar structure possess high potential for pseudocapacitance and promote charge storage due to its variable oxidation states (from +2 to +6). Also, the weak intermolecular van der Waals interactions between the layers allow proper electrolyte diffusion and structural rigidity resulting in high electrochemical stability [211,212]. Different architectures of MoS_2 have been examined for supercapacitor electrodes in literature. The ultrathin layers enable large surface area, porosity and significant active edge sites in MoS_2 nanostructures, which may lead to enhanced electrochemical activity using different morphology of MoS_2 [187], [213]. These properties of MoS_2 nanostructures can be utilized for electrode materials in supercapacitors. Different

phases (1T or 2H) and nanostructures like nanoparticles, nanosheets etc. are being explored for improving the performance of supercapacitors. The specific capacitances in the range 100 to 150 F g^{-1} were reported in literature for different MoS_2 nanostructures based supercapacitors with different aqueous electrolytes [114], [193]. Hu and co-worker synthesized tubular C-MoS_2 nanostructure, exhibiting a maximum capacitance value of 210 F g^{-1} at a discharge current density of 1 A g^{-1} [214]. Few reports suggested high specific capacitance of MoS_2 nanostructures in the range 400-600 F g^{-1} with aqueous electrolyte at a prolonged scan rate of 1 mV s^{-1}, which drastically drops to a lower range 50-200 F g^{-1} at a higher scan rate of 100 mV s^{-1} [215,216].

In the present chapter, we have demonstrated hydrothermally prepared reduced graphite oxides, hexagonal phase of MoS_2 nanostructures and MoS_2-rGO heterostructure as suitable electrode materials for supercapacitor applications. We have examined the suitability of rGO and MoS_2 based electrodes with both acidic and neutral aqueous electrolytes. We have optimized the high capacitive performance of rGOs based electrodes prepared with hydrazine hydrate (HH) and urea as reducing agents at low temperatures (~100 °C). We have investigated the pristine 2H-MoS_2 nanosheets and nanoflowers based electrodes for supercapacitor, showing improved capacitive behaviour in acidic and neutral electrolytes. We have also demonstrated the capacitive performance of MoS_2-rGO heterostructure supercapacitor in both electrolytes.

4.2 Results and Discussion

In this section, we have discussed three-cell configuration electrochemical analysis of different rGOs and MoS_2 nanostructures, prepared in this thesis work. We have investigated the suitability of respective electrodes for double layer capacitance and

pseudocapacitance in acidic and neutral electrolytes. The specific capacitance of electrodes using CV curve can be determined using the following **equation 4.1** [177]-

$$C_s = \frac{Area\ under\ the\ cyclic\ voltammetry\ curve}{Mass\ of\ electrode\ material \times Potential\ window \times Voltage\ scan\ rate} \quad (4.1)$$

The specific capacitance (C_s) value from GCD curve can be calculated using following **equation 4.2-**

$$C_s = \frac{Current \times Discharge\ time}{Mass\ of\ the\ electrode \times Potential\ window} \quad (4.2)$$

4.2.1 Reduced Graphite Oxides for Supercapacitors Application

In this study, we have optimized the capacitive performance of rGOs prepared with hydrazine hydrate (rGO-HH) and urea (rGO-Urea) at low temperature (100 °C). This section deals with the electrochemical characterization of hydrothermally synthesized rGO-HH and rGO-Urea-based electrodes. The cyclic voltammetry (CV), galvanostatic charge-discharge (GCD) and impedance spectroscopy (EIS) techniques have been performed for rGO nanostructures-based electrodes. The structural, vibrational and morphological characterizations of rGO-HH and rGO-Urea have already been discussed in section 3.3.1.1. of chapter 3. To evaluate the capacitive behaviour, we have performed CV and GCD measurements for rGO-HH and rGO-Urea coated carbon paper electrodes in neutral (1M Na_2SO_4) and acidic electrolyte (1M H_2SO_4) using a three-electrode configuration in potential range of 0 to 1 V.

4.2.1.1 Capacitance Study of rGO-HH Electrodes

Figure 4.3 (a) shows the CV curves for rGO-HH electrodes in neutral electrolyte (1M Na_2SO_4). It is showing specific capacitances of 80, 75, 62, 50 and 40 F g^{-1} for rGO-HH electrode at the voltage sweep rate of 5, 10, 20, 50 and 100 mV s^{-1} neutral electrolyte.

Further, we have performed the GCD measurements for better understanding and quantitative insight of charging discharging capability of rGO-HH based electrodes.

The rGO-HH electrodes show poor capacitance of 19 and 11 F g^{-1} at discharge current density of 1 and 2 A g^{-1} in neutral electrolyte, as shown in **Figure 4.3 (b)**. The poor capacitive behaviour is due to the sluggish diffusion of Na^+ ions in rGO-HH. **Figure 4.3 (c)** and **(d)** shows capacitive behaviour of rGO-HH coated conducting carbon electrodes in acidic (1M H_2SO_4) electrolyte. **Figure 4.3 (c)** shows CV curves for rGO-HH electrodes in acidic electrolyte at different voltage scan rates. A large area of parallelogram for rGO electrodes suggests the excellent capacitive behaviour. The specific capacitances of 286, 283, 277 and 277 F g^{-1} are observed at the voltage sweep rates of 10, 20, 50 and 100 mV s^{-1}, respectively, confirming the excellent capacitive behaviour of the electrode. The presence of oxygen-containing functional groups results in redox behaviour of rGO-HH and hence deviation from rectangular shape is observed [217, 218]. The nature of the CV curve is not deformed even at the higher scan rate for both rGO-HH, indicating the better sustainability of capacitive behaviour. A larger capacitance of rGO-HH can be associated with higher surface area and better reduction of epoxides. This behaviour can be attributed to the presence of larger and uniform sp^2 network in rGO-HH and hence better conductivity. The GCD curves of rGO-HH electrode at different current densities ranging from 1 to 4 A g^{-1} are shown in **Figure 4.3 (d)** for acidic electrolyte. The near triangular behaviour confirms the reversible charging-discharging characteristics of rGO-HH samples for supercapacitor application [160]. The specific capacitance values of 300, 286 and 260 F g^{-1} are observed at discharge current densities of 1, 2 and 4 A g^{-1} for rGO-HH.

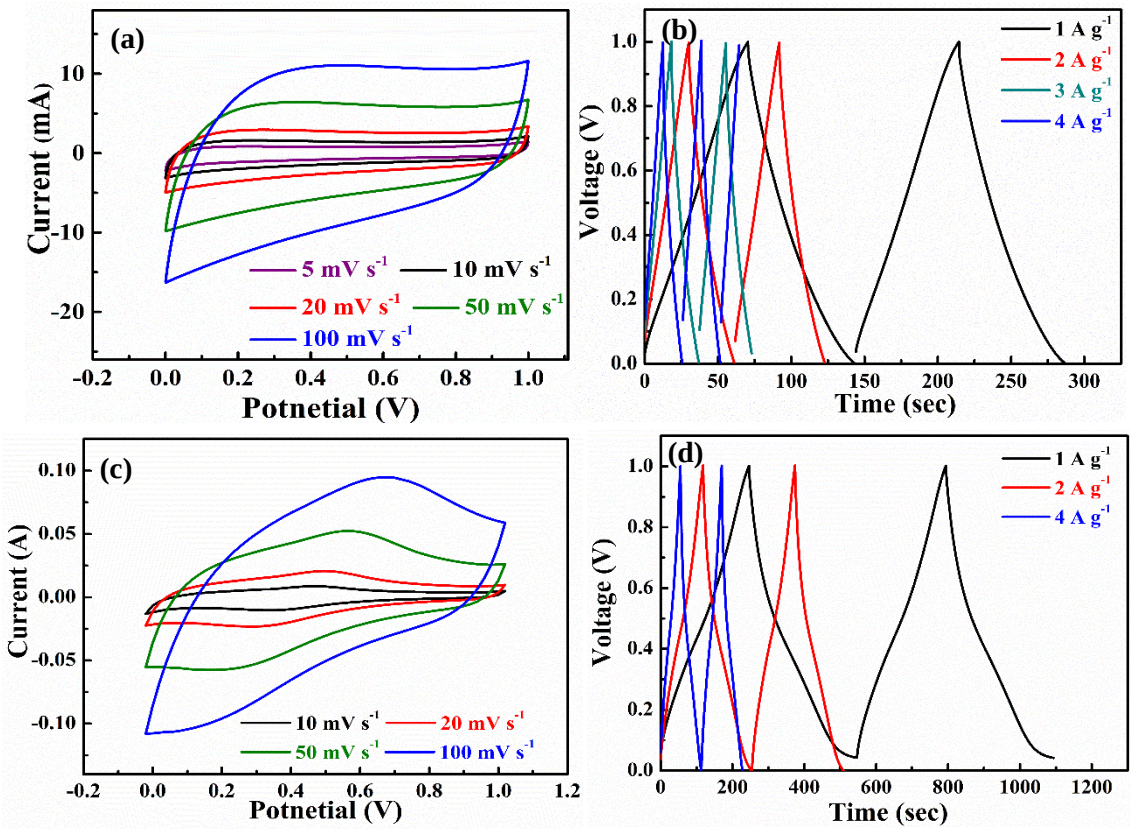

Figure 4.3 *Electrochemical measurements for rGO-HH electrode* ***(****a) CV curves at different scan rates and (b) GCD curves at different discharge current densities with 1M Na_2SO_4 electrolyte; (c) CV curves at different scan rates and (d) GCD curves at different discharge current densities with 1M H_2SO_4 electrolyte.*

To further understand the kinetics of rGO-HH electrode at electrode/electrolyte interface, we have performed EIS study in both aqueous electrolytes. **Figure 4.4 (a)** displays Nyquist plots for rGO-HH electrode fitted using constant phase element (CPE) equivalent circuit. The solution resistance (R_s) in the equivalent circuit indicates the resistance of the electrolyte combined with the internal resistance of the electrode. The smaller value of solution resistance (R_s) of rGO-HH (R_s ~0.9 Ω) in acidic compared to neutral media (R_s ~2.2 Ω) indicate ease in combination of H^+ ion with rGO-HH electrode.

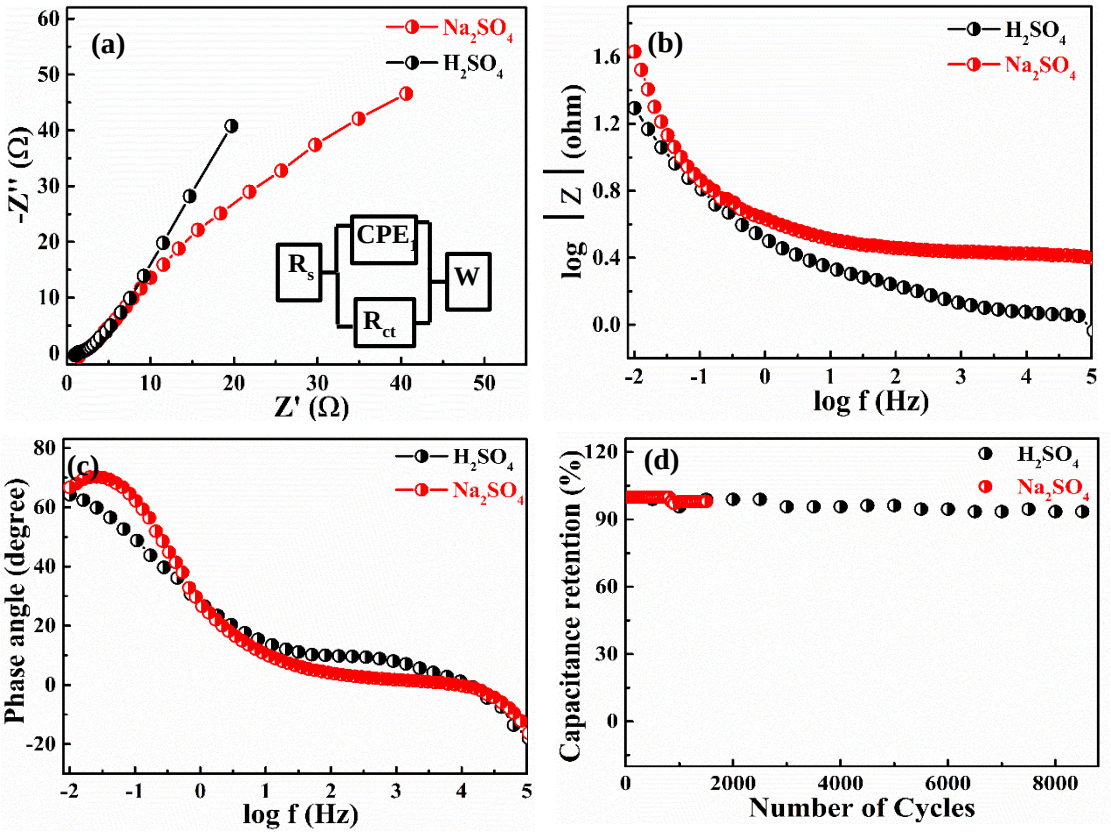

Figure 4.4 *Electrochemical measurements for rGO-HH electrode* ***(****a) Nyquist plots (inset shows the equivalent circuit), (b)Bode impedance plots and (c) Bode phase plots and (d) Cyclic stability test at 100 mV* s^{-1} *in neutral and acidic electrolytes.*

The rate of redox reactions at electrode/electrolyte interface is determined using charge transfer resistance (R_{CT}). The smaller R_{CT}~ 4.8 Ω value in acidic medium compared to (R_{CT}~ 6.5 Ω) in neutral one suggests fast ion transport at electrode/electrolyte interface in acidic electrolyte. **Figure 4.4 (b)** shows Bode impedance plots [log |Z| vs. log f], which followed the trend of Nyquist plot and provides the direct view of impedance (modulus) for each frequency range. It clearly indicates low value of |Z|, suggesting good conducting behaviour of rGO-HH in both electrolytes. The Bode phase plots of **Figure 4.4 (c)** show the maximum phase angle ~ 68° and 64° for neutral and acidic electrolytes, respectively, indicates the presence of pseudocapacitive behaviour along with EDLC for rGO-HH due to the presence of oxygen containing functional groups. We have further investigated the stability of rGO-HH electrode for 8500 and 1500 cycles in acidic and neutral electrolyte,

respectively at a scan rate of 100 mV s^{-1}, as shown in **Figure 4.4 (d)**. The maximum capacitance retentions of 95.8% after 8500 cycles and 98% after 1500 cycles have been observed for rGO-HH electrode in acidic and neutral electrolyte.

4.2.1.2 Capacitance Study of rGO-Urea Electrodes

We have also investigated the capacitive behaviour of rGO-Urea coated carbon paper electrodes in neutral (1M Na_2SO_4) and acidic (1M H_2SO_4) electrolytes using a three-electrode configuration in the potential range 0 to 1 V. **Figure 4.5 (a)** shows the CV curves for rGO-Urea electrodes in neutral electrolyte (1M Na_2SO_4) indicating low specific capacitances of 12, 10, 7, 5 and 5 F g^{-1} at the voltage sweep rates of 5, 10, 20, 50 and 100 mV s^{-1}, respectively. Further, GCD measurements confirm the poor charging discharging capability of rGO-Urea electrode in neutral electrolyte with poor capacitance~ 2 and 1 F g^{-1} at discharge current densities of 1 and 2 A g^{-1}, as shown in **Figure 4.5 (b)**. The poor capacitive behaviour is due to the highly sluggish diffusion of Na^+ ions in rGO-Urea. **Figure 4.5 (c)** shows the CV curves for rGO-Urea electrodes in 1 M H_2SO_4 at different scan rates. A large area of parallelogram for rGO-Urea electrodes suggests good capacitive behaviour. The specific capacitances of 212, 160, 277 and 139 F g^{-1} are observed at the voltage sweep rates of 10, 20, 50 and 100 mV s^{-1}, respectively, confirming the good capacitive behaviour of the electrode. The presence of oxygen-containing functional groups results in redox behaviour of rGO samples and hence deviation from rectangular shape is observed. The nature of the CV curve is well maintained even at the higher scan rate, indicating the better sustainability of capacitive behaviour. The GCD curves of rGO-Urea electrode at different current densities ranging from 1 to 4 A g^{-1} are shown in **Figure 4.5 (d)** for acidic electrolyte, showing the near triangular behaviour and reversible charging-discharging characteristics of rGO-Urea for supercapacitor application. The specific

capacitance values of 220, 196 and 176 F g^{-1} are observed at discharge current densities of 1, 2 and 4 A g^{-1} for rGO-urea, respectively.

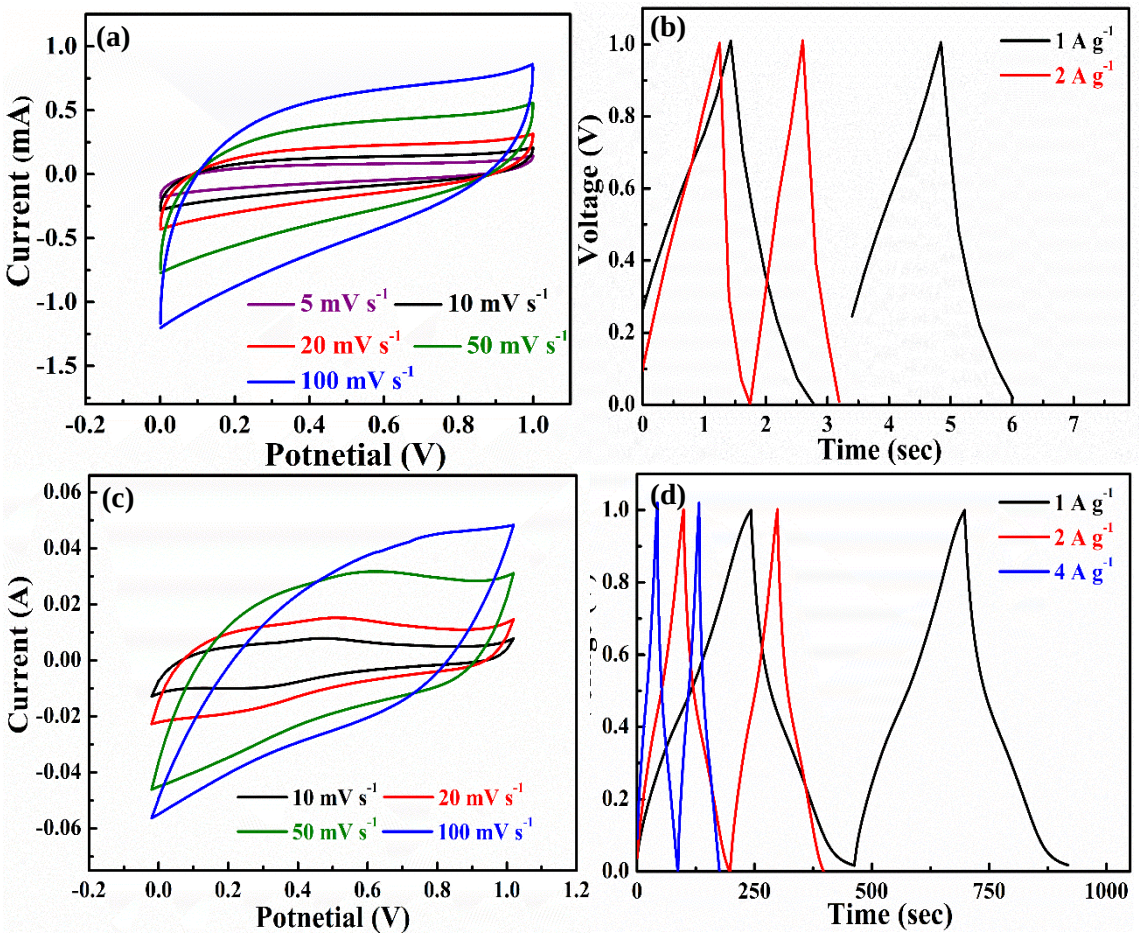

Figure 4.5 *Electrochemical measurements for rGO-Urea electrode (a) CV curves at different scan rates and (b) GCD curved at different discharge current densities in 1M Na_2SO_4 electrolyte; (c) CV curves at different scan rates and (d) GCD curves at different discharge current densities in 1M H_2SO_4 electrolyte.*

To further understand the kinetics of rGO-Urea electrode at electrode/electrolyte interface, we have performed EIS study in both aqueous electrolytes. **Figure 4.6 (a)** displays Nyquist plots for rGO-Urea electrode fitted using CPE equivalent circuit. The smaller value of solution resistance (R_s) of rGO-Urea (R_s ~1.9 Ω) in acidic compared to neutral media (R_s ~2.4 Ω) indicate ease in diffusion of H^+ ion in rGO-Urea electrode. The smaller R_{CT} ~ 14.2 Ω value in acidic medium compared to R_{CT} ~ 755 Ω in neutral one suggests fast ion transport at electrode/electrolyte interface in acidic electrolyte.

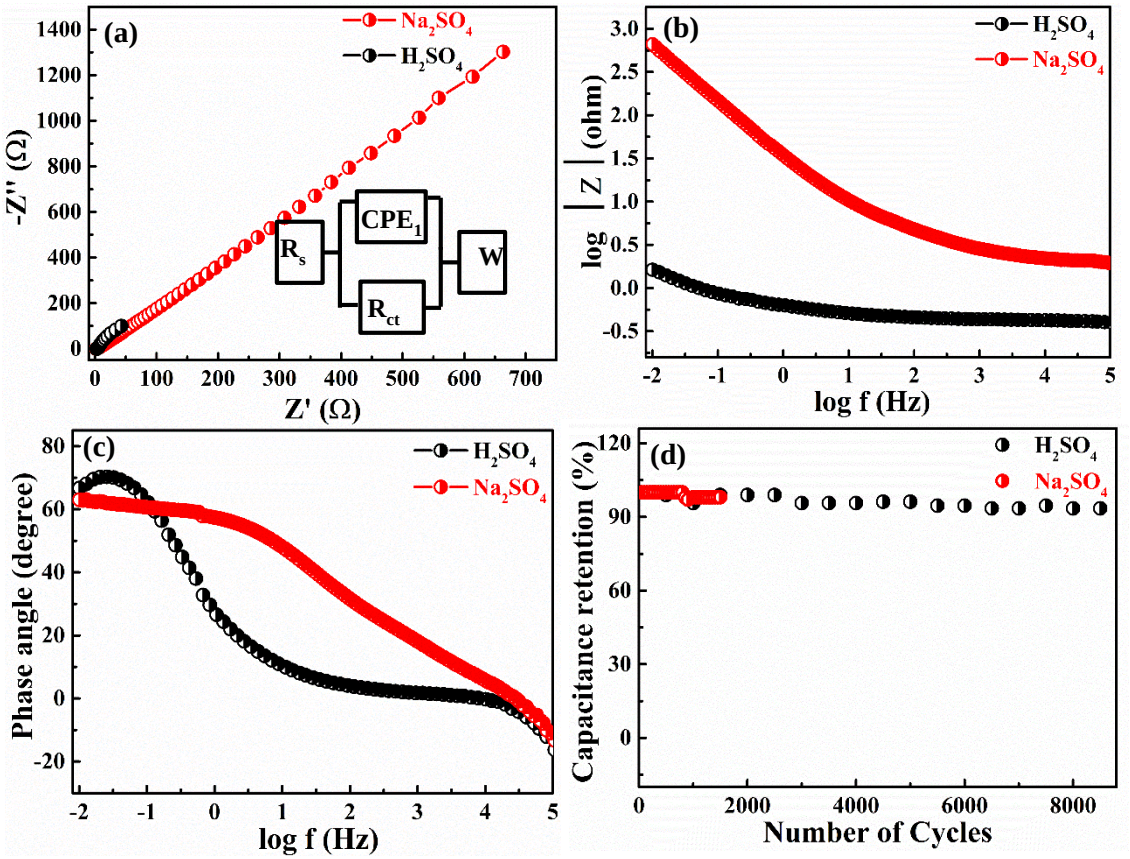

Figure 4.6 *Electrochemical measurements for rGO-Urea electrode* ***(****a) Nyquist plots (inset shows the equivalent circuit), (b) Bode impedance plots (c) Bode phase angle plots and (d) Cyclic stability test in neutral and acidic electrolytes.*

Figure 4.6 (b) shows Bode impedance plots [log |Z| vs. log f] indicating lower impedance of rGO-Urea in acidic electrolyte compared to neutral electrolyte suggesting better conducting behaviour of electrode in acidic medium. The Bode phase plots of **Figure 4.6 (c)** show the maximum phase angle~ 63 and 66° in neutral and acidic medium, suggesting presence of pseudocapacitive behaviour along with EDLC in rGO-Urea. The slope of Bode phase plot in acidic medium suggest occurrence of faster process at electrode/electrolyte interface. We have further investigated the stability of rGO-Urea electrode for 8500 cycles in acidic electrolyte and for 1500 cycles in neutral electrolyte at a scan rate of 100 mV s^{-1}, as shown in **Figure 4.6 (d)**. The maximum capacitance retentions of 93.5% after 8500 cycles and 96 % after 1500 cycles have been observed for rGO-Urea electrode.

Therefore, studied electrochemical tests clearly indicate that the rGOs electrodes show better and more sustainable capacitive performance in the acidic electrolyte compared to neutral one due to ease of diffusion of H^+ ion compared to Na^+ ion in rGO samples. Hence, better removal of epoxides, better electrical conductivity along with the presence of larger surface area and uniform sp^2 network in rGO-HH compared to rGO-Urea leads to the better capacitive behaviour of rGO-HH electrodes.

4.2.2 MoS_2 Nanoflowers Electrodes for Supercapacitor Application

In this study, we have observed the capacitive performance of MoS_2 nanoflowers electrodes. This section deals with the investigation of the capacitive behaviour of MoS_2 nanoflowers-based electrodes by performing CV, GCD and EIS studies in acidic and neutral electrolytes using three electrode configurations. The characterization of MoS_2 nanoflowers has already been discussed in section 3.3.3.1. of chapter 3. We have performed the electrochemical studies for MoS_2 nanoflowers coated carbon paper electrodes in neutral (1M Na_2SO_4) and acidic electrolyte (1M H_2SO_4) using a three-electrode configuration in potential range -0.7 to 0.2 V for neutral electrolyte and -0.3 to 0.4V for acidic electrolyte. **Figure 4.7 (a)** shows the CV curves for MoS_2 nanoflowers electrodes in the neutral electrolyte at different voltage scan rates. A large area of parallelogram for MoS_2 nanoflowers electrodes suggests the excellent capacitive behaviour of MoS_2 nanoflowers. The maximum specific capacitances of 354 F g^{-1} is observed for MoS_2 nanoflowers at 10 mV s^{-1}. The absence of any redox peak in CV curves for MoS_2 nanoflowers indicates purely the formation of electrical double-layer at electrode-electrolyte interface, as observed in other reports [219,220]. The maximum specific capacitance of 227 F g^{-1} was obtained at higher scan rate of 100 mV s^{-1}, suggesting high degree of sustainability of capacitive performance of MoS_2 nanoflowers in neutral medium. The capacitive characteristic is also measured by a constant current charge-discharge cyclic

test, which gives better quantitative insight into the capacitive performance of electrode material. **Figure 4.7 (b)** depicts the GCD curves at different current densities of 1, 2, 3 and 4 Ag^{-1}. The reversible charge-discharge characteristics of MoS_2 nanoflowers attribute to the quasi-triangular behaviour and high columbic efficiency. It shows the specific capacitance of 382 F g^{-1} at discharge current density of 1 A g^{-1}. The higher value of specific capacitance can be attributed to the accessible surface area between well separated petals of flower structure and presence of functional groups which may increase the wettability of electrode for easy transport of electrolyte. The MoS_2 nanoflowers electrodes show high retention (~ 70 %) in specific capacitance (~ 271 F g^{-1}) even at very high discharge current density of 4 A g^{-1} indicating high-rate performance of MoS_2 nanoflowers electrode.

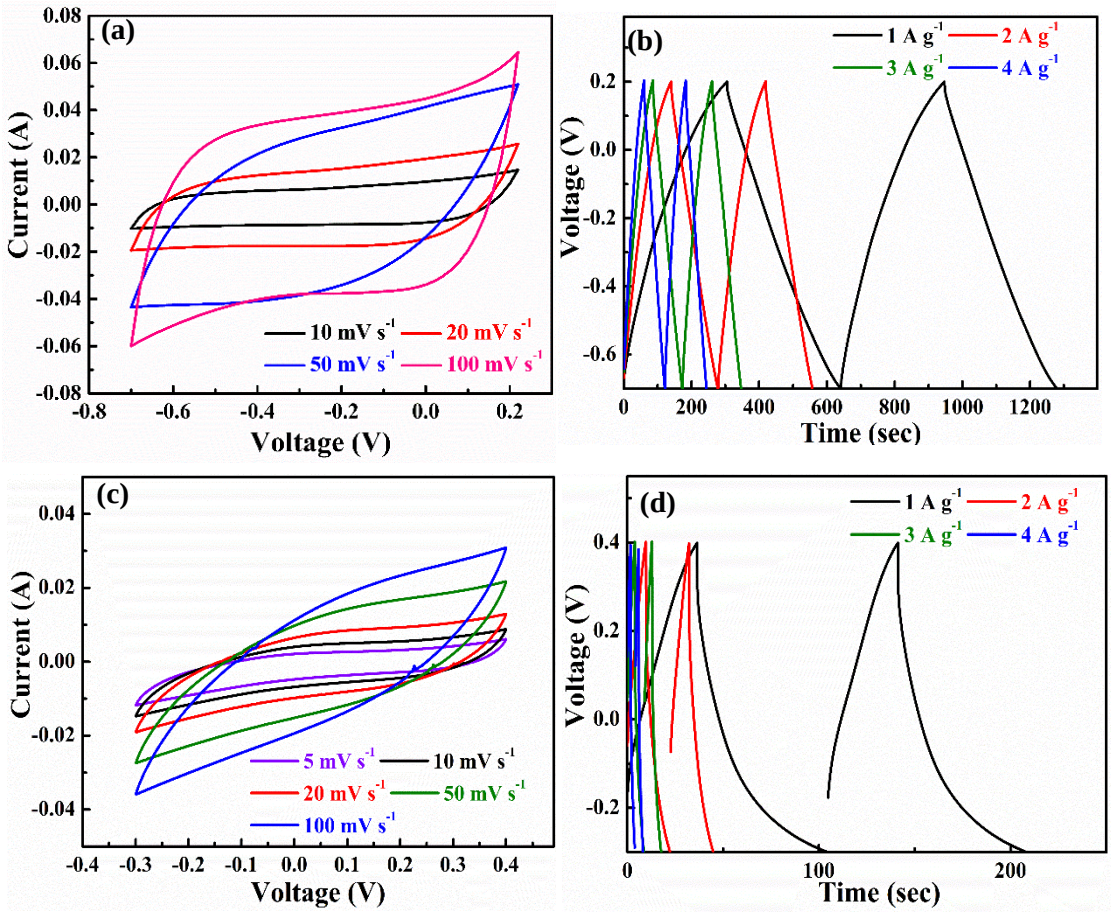

Figure 4.7 *Electrochemical measurements for MoS_2 nanoflowers electrode (a) CV curves at different scan rates and (b) GCD curves at different discharge current densities in 1M Na_2SO_4 electrolyte; (c) CV curves at different scan rates and (d) GCD curves at different discharge current densities in 1M H_2SO_4 electrolyte.*

Figure 4.7 (c) and **4.7 (d)** represents capacitive behaviour of MoS_2 nanoflowers electrode in acidic electrolyte. The CV curves of **Figure 4.7 (c)** exhibit slight divergence from symmetric rectangular shape, which indicates possibility of more faradic reactions at electrode/electrolyte interface. The maximum specific capacitance of 116 F g^{-1} has been obtained at a sweep rate of 5 mV s^{-1}, which is much lower compared to capacitance in neutral electrolyte. The GCD curves of MoS_2 nanoflowers electrodes at different current densities ranging from 1 to 4 A g^{-1} are shown in **Figure 4.7 (d)** for acidic electrolyte, which clearly show the deviation from triangular behaviour. The specific capacitance of 68, 25, 14, and 9 F g^{-1} are obtained at discharge current density of 1, 2, 3, and 4 A g^{-1}, respectively, showing poor capacitive sustainability of electrode in acidic electrolyte.

Further we have studied the MoS_2 nanoflowers electrode kinetics by EIS study in both electrolytes. **Figure 4.8 (a)** displays Nyquist plots for MoS_2 nanoflowers electrode fitted using CPE equivalent circuit. The presence of semicircle at higher frequencies and a straight line at the lower frequency region confirms the capacitive behaviour of MoS_2 nanoflowers electrode. The lower R_s value is observed for acidic electrolyte (0.8 Ω) compared to neutral one (2.0 Ω) due to the small ionic size of the H^+ ion. The smaller value R_{CT} ~ 3.4 Ω value for neutral electrolyte compared to acidic electrolyte (R_{CT}~ 20 Ω), indicates better charge transfer at electrode/electrolyte interface in neutral electrolyte. The Nyquist plots of MoS_2 nanoflowers show nearly a vertical line parallel to the imaginary axis at low frequency, indicating excellent capacitance response of MoS_2 nanoflowers electrode in neutral electrolyte. **Figure 4.8 (b)** shows Bode impedance plots which followed the trend of Nyquist plot and provides the direct view of impedance (modulus) for each frequency range. It clearly shows low impedance values for MoS_2 nanoflowers in both electrolytes. The Bode phase plots of **Figure 4.8 (c)** show the maximum phase angle ~ 70° and 55° in neutral and acidic medium, suggesting pseudocapacitive predominant

behaviour for charge storage process for MoS_2 nanoflowers in acidic electrolyte. However, low capacitance in acidic electrolyte is observed because of low capacitive potential window arising due to catalytic activity of MoS_2 nanoflowers in acidic medium.

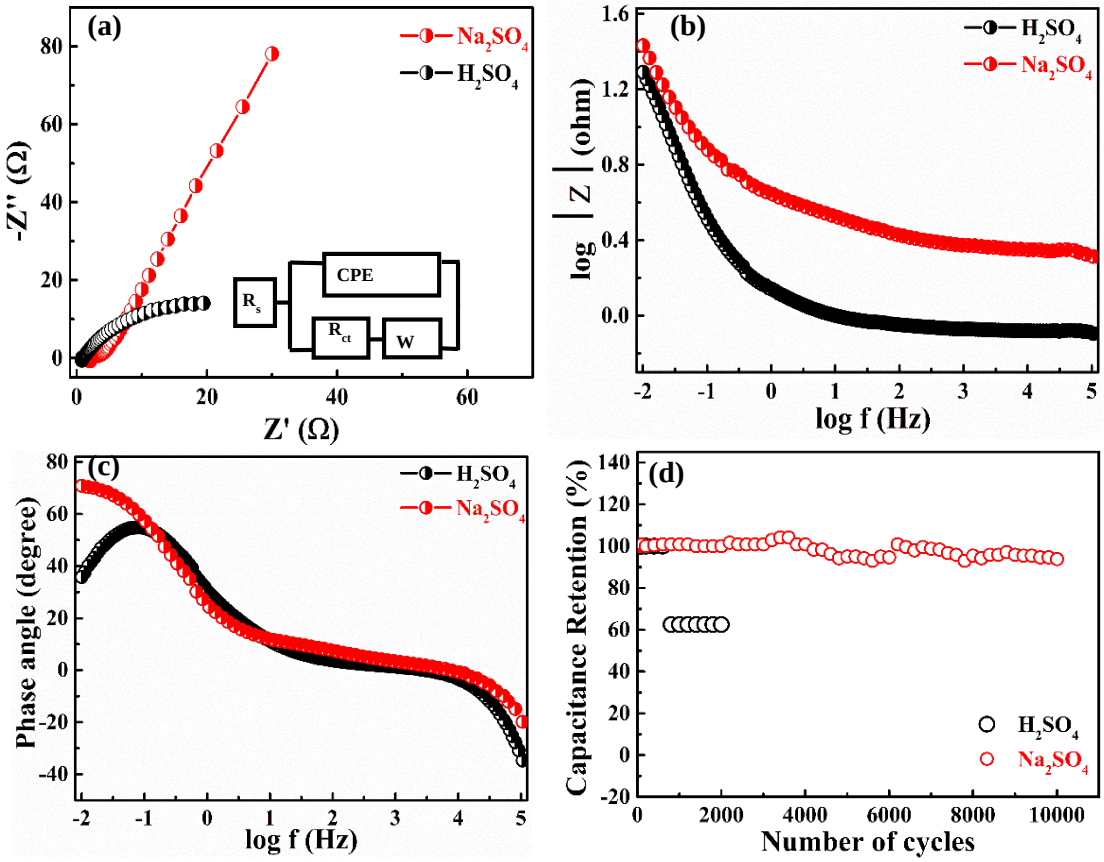

Figure 4.8 *Electrochemical measurements for MoS_2 nanoflowers electrode (a) Nyquist plots (inset shows the equivalent circuit), (b) Bode impedance plots, (c) Bode phase angle plots, and (d) Cyclic stability test at 100 mV s^{-1} scan rate in neutral and acidic electrolytes.*

Figure 4.8 (d) shows long-term durability of capacitive performance of MoS_2 nanoflowers electrode tested at a scan rate of 100 mV s^{-1} for neutral and acidic electrolytes, respectively. Initial 2000 cycles show 100% capacitance retention in neutral electrolyte and enhancement in capacitance is observed after 2000 cycles due to probable activation process of the supercapacitor electrode in neutral electrolyte. The maximum capacitance retention of nearly 94% and 62.5 % is observed after 10000 and 2000 cycles for neutral and acidic electrolytes, respectively, suggesting higher stability of MoS_2 nanoflowers electrode

for the neutral electrolyte. In summary, the electrochemical study comprising CV, GCD, EIS and stability test measurements verify that the prepared 2H phase MoS_2 nanoflowers show excellent capacitive behaviour along with good cyclic stability in neutral electrolyte. It also shows significant performance in acidic electrolyte as well. The present work suggests the improved and sustained capacitive performance of 2H-MoS_2 nanoflowers electrode is due to the presence of exposed edges during petal formation in flower like structure.

4.2.3 MoS_2 Nanosheets Electrodes for Supercapacitor Application

This section deals with the investigation of the capacitive performance of MoS_2 nanosheets-based electrodes in three cell electrochemical configuration, using CV, GCD and EIS studies. The characterization of MoS_2 nanosheets has been discussed in section 3.3.4.1. of chapter 3. To evaluate the capacitive behaviour, we have performed CV and GCD measurements for MoS_2 nanosheets electrodes in neutral (1M Na_2SO_4) and acidic (1M H_2SO_4) electrolytes in potential range -0.7 to 0.2 V for neutral electrolyte and -0.3 to 0.4 V acidic electrolyte. **Figure 4.9 (a)** demonstrates CV curves of MoS_2 nanosheets electrodes in the neutral electrolyte at varied voltage sweep rates from 5 to 100 mV s^{-1}. The broad area of the parallelogram of MoS_2 nanosheets electrodes indicates promising capacitive behaviour. In the neutral electrolyte, the presence of a small pseudo peak at low sweep rates in the CV curve of the MoS_2 nanosheets electrodes implies the formation of electrical double-layer (EDL) with some order of pseudocapacitance. At higher sweep rates, the current density gradually increases while shape of CV curve remains almost near rectangular, suggesting sustainable double layer capacitance behaviour of MoS_2 nanosheets electrodes. It shows the specific capacitance of 277, 204, 127, 53 and 27 F g^{-1} at the voltage sweep rates of 5, 10, 20, 50 and 100 mV s^{-1}, respectively, confirming the excellent capacitive behaviour of the electrode.

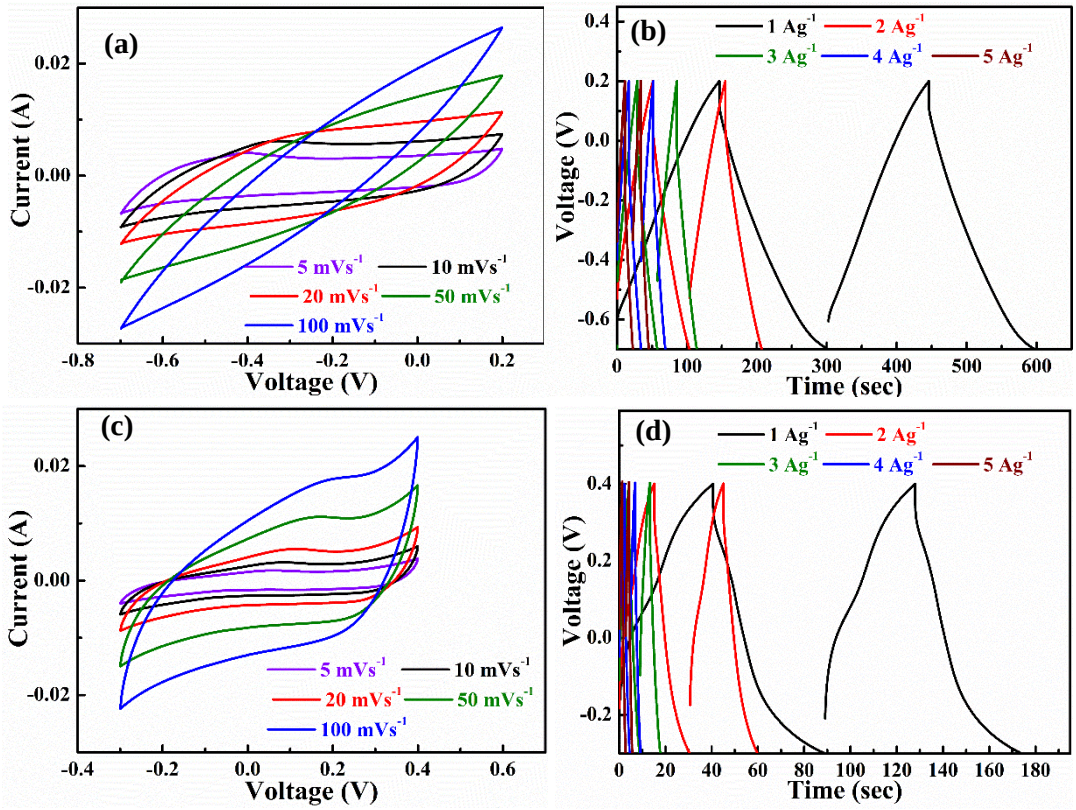

Figure 4.9 *Electrochemical measurements for MoS_2 nanosheets electrode (a) CV curves at different scan rates, and (b) GCD curves at different discharge current densities in 1M Na_2SO_4 electrolyte; (c) CV curves at different scan rates, and (d) GCD curves at different discharge current densities in 1M H_2SO_4 electrolyte.*

Further, we have performed the GCD measurements for better understanding and quantitative insight of charging discharging capability of MoS_2 nanosheets electrodes in neutral electrolyte. The GCD curves of MoS_2 nanosheets electrodes at different current densities ranging from 1 to 5 A g^{-1} are given in **Figure 4.9 (b)**. The triangular behaviour of charge-discharge characteristics for MoS_2 nanosheets electrodes suggests excellent columbic efficiency. The specific capacitances of 173, 117, 93,76 and 63 F g^{-1} are obtained at discharge current densities of 1, 2, 3, 4 and 5 A g^{-1}, respectively. The excellent capacitive behaviour of MoS_2 nanosheets can be attributed to the accessible electrochemical active surface area between wrinkled sheets and presence of functional groups that enhances the wettability of electrode, resulting in the easy transport of electrolyte and may also take part is redox process. The decrement in specific capacitance with increasing sweep rate may be

attributed to the reduced adsorption of ions in a short duration at pores of MoS_2 nanosheets. **Figure 4.9 (c)** and **4.9 (d)** represents capacitive behaviour of MoS_2 nanosheets electrodes in acidic electrolyte. The CV curves of **Figure 4.9 (c)** depict divergence from a symmetric rectangular shape, which shows more charge transfer and faradic reactions are occurring at the electrode/electrolyte interface. The specific capacitance of 93, 76, 62, 45 and 33 F g^{-1} has been obtained at voltage sweep rates of 5, 10, 20, 50 and 100 mV s^{-1}, which is lower compared to the neutral electrolyte. The GCD curves of MoS_2 nanosheets electrodes at different current densities ranging from 1 to 5 A g^{-1} are shown in **Figure 4.9 (d)** for acidic electrolyte, which clearly show the deviation from triangular behaviour. The specific capacitances of 62, 40, 21, 17 and 7 F g^{-1} are obtained at discharge current densities of 1, 2, 3, 4 and 5 A g^{-1}, respectively, showing poor capacitive sustainability of electrode in acidic electrolyte.

To further understand the kinetics at electrode/electrolyte interface, we have performed EIS study in both aqueous electrolytes. **Figure 4.10 (a)** displays Nyquist plots for MoS_2 nanosheets electrodes, fitted with CPE equivalent circuit as displayed in the inset. The solution resistance (R_s) in the equivalent circuit indicates the resistance of the electrolyte combined with the internal resistance of the electrode, which is generally lower for acidic electrolytes compared to neutral electrolytes due to the small ionic size of the H^+ ion. The present MoS_2 nanosheets electrode shows R_s values of 6.0 and 0.8 Ω for neutral and acidic electrolyte, respectively. The rate of redox reactions at the electrode/electrolyte interface is determined using charge transfer resistance (R_{CT}). The smaller value of R_{CT}~ 3.0 Ω for neutral electrolyte compared to acidic electrolyte (R_{CT}~ 5.3 Ω), suggests fast ion transport at electrode/ electrolyte interface in neutral medium. The shorter diffusion path of MoS_2 nanosheets electrode in neutral electrolyte depicts enhanced capacitive behaviour. The

CPE_L is a constant phase element that represents double-layer capacitance, which arises at solid-ionic solution interfaces due to ionic and/or electronic charge separation [221,222].

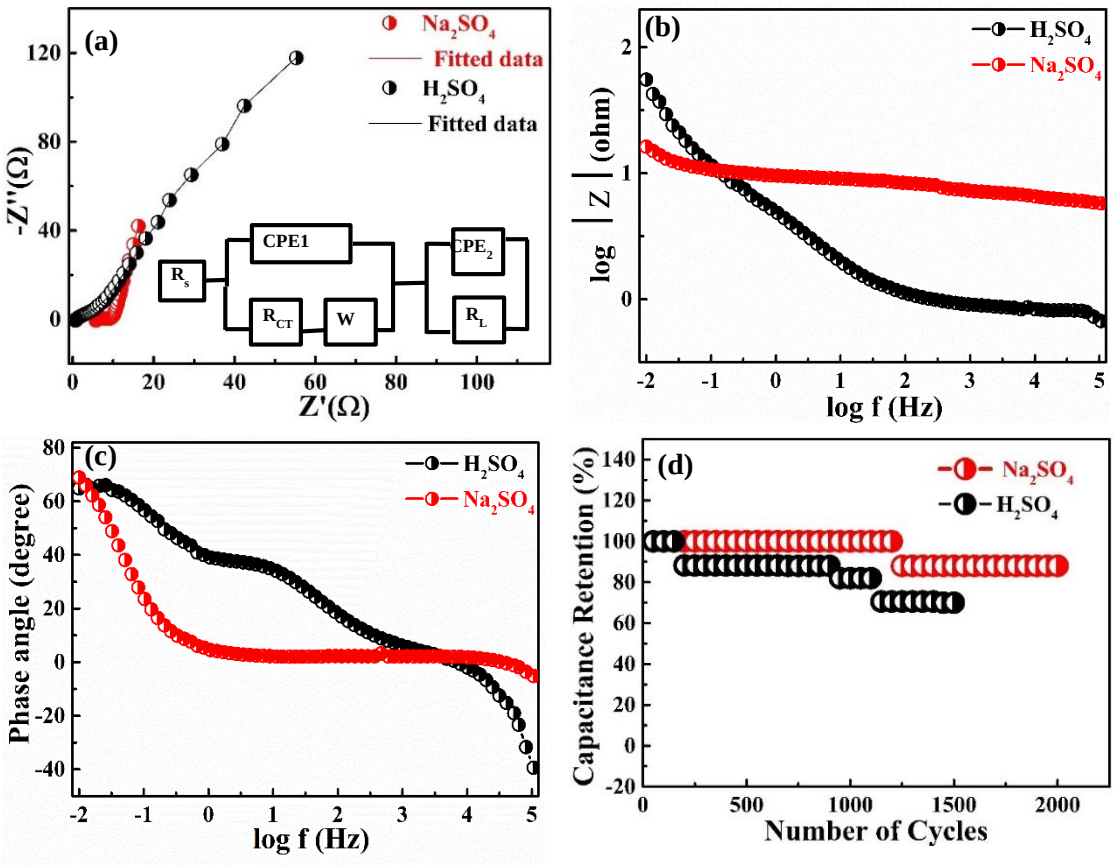

Figure 4.10 *Electrochemical measurements for MoS_2 nanosheets electrode (a) Nyquist plots (inset shows the equivalent circuit), (b) Bode impedance plots, (c) Bode phase plots and (d) Cyclic stability test at a discharge current density of 5 A g^{-1}in neutral and acidic electrolytes.*

The Bode plots of **Figure 4.10 (b)** clearly indicate the lower impedance of MoS_2 nanosheets in neutral electrolyte compared to acidic one suggesting better conductivity of electrode in neutral electrolyte. The Bode phase plots of **Figure 4.10 (c)** show the maximum phase angle ~ 68° and 65° in neutral and acidic medium, suggesting pseudocapacitive predominant behaviour for charge storage process for MoS_2 nanosheets in both electrolytes. We further investigated the stability of MoS_2 nanosheets electrodes for supercapacitor application. **Figure 4.10 (d)** shows long-term durability of capacitive behaviour of MoS_2 nanosheets electrodes tested at a discharge current density of 5 A g^{-1} for neutral and acidic electrolytes. The maximum capacitance retention of nearly 88 % and

70% are observed after 2000 and 1500 cycles for neutral and acidic electrolytes, respectively, suggesting higher stability of MoS_2 nanosheets electrode in neutral electrolyte.

In summary, the electrochemical study comprising CV, GCD measurements, stability test and EIS measurements verify that the prepared 2H phase MoS_2 nanosheets electrode shows better pseudocapacitive response and stability in neutral electrolyte compared to acidic one. The good electrochemical performance in this study is attributable to the availability of functional groups and exposed edges due to the well-separated sheet of synthesized MoS_2. The lower capacitive behaviour of MoS_2 nanosheets electrode in acidic medium could be due to high degree of catalytic effect of MoS_2 with H^+ ion that reduces the potential window dramatically and hence the capacitance [223]. The high capacitance performance in neutral electrolyte of as synthesized MoS_2 nanosheets electrodes suggests their suitability for the development of efficient supercapacitor devices.

4.2.4 MoS_2-rGO Heterostructures Electrodes for Supercapacitor Application

After examining capacitive behaviour of rGO and MoS_2 nanostructures, we have investigated the capacitive performance of in situ hydrothermally synthesized nanosheets of MoS_2-rGO heterostructure. The characterization of MoS_2-rGO heterostructure has been discussed in section 3.3.5.1. of chapter 3. This section deals with the investigation of electrochemical activity MoS_2-rGO heterostructure coated carbon paper electrodes using CV, GCD and EIS studies with three-electrode configuration in potential range of -0.8 to 0.2 V for neutral (1M Na_2SO_4) and -0.3 to 0.4V for acidic(1M H_2SO_4) electrolytes. **Figure 4.11 (a)** shows the CV curves for MoS_2-rGO heterostructure electrodes in neutral electrolyte at different voltage scan rates. Large area of a parallelograms for heterostructure electrode suggest good capacitive behaviour. The specific capacitances of 171, 152, 128, 99 and 74 F g^{-1} are observed at voltage sweep rate of 5, 10, 20, 50 and 100 mV s^{-1} for MoS_2-

rGO heterostructure electrode. The deviated rectangular behaviour of CV curves suggests the presence of double layer capacitance and pseudocapacitance. **Figure 4.11 (b)** depicts the GCD curves of heterostructure at discharge current densities of 1, 2, 3, 4 and 5 A g^{-1}. The GCD characteristics of heterostructure attribute the quasi-triangular behaviour and high columbic efficiency again suggesting presence of pseudocapacitance and double layer capacitance. The specific capacitances of 136, 85, 72, 59 and 55 F g^{-1} are obtained at discharge current densities of 1, 2, 3, 4 and 5 A g^{-1}, respectively. The lower value of specific capacitance in neutral electrolyte can be attributed to the dominance of rGO sheets over MoS_2 nanosheets.

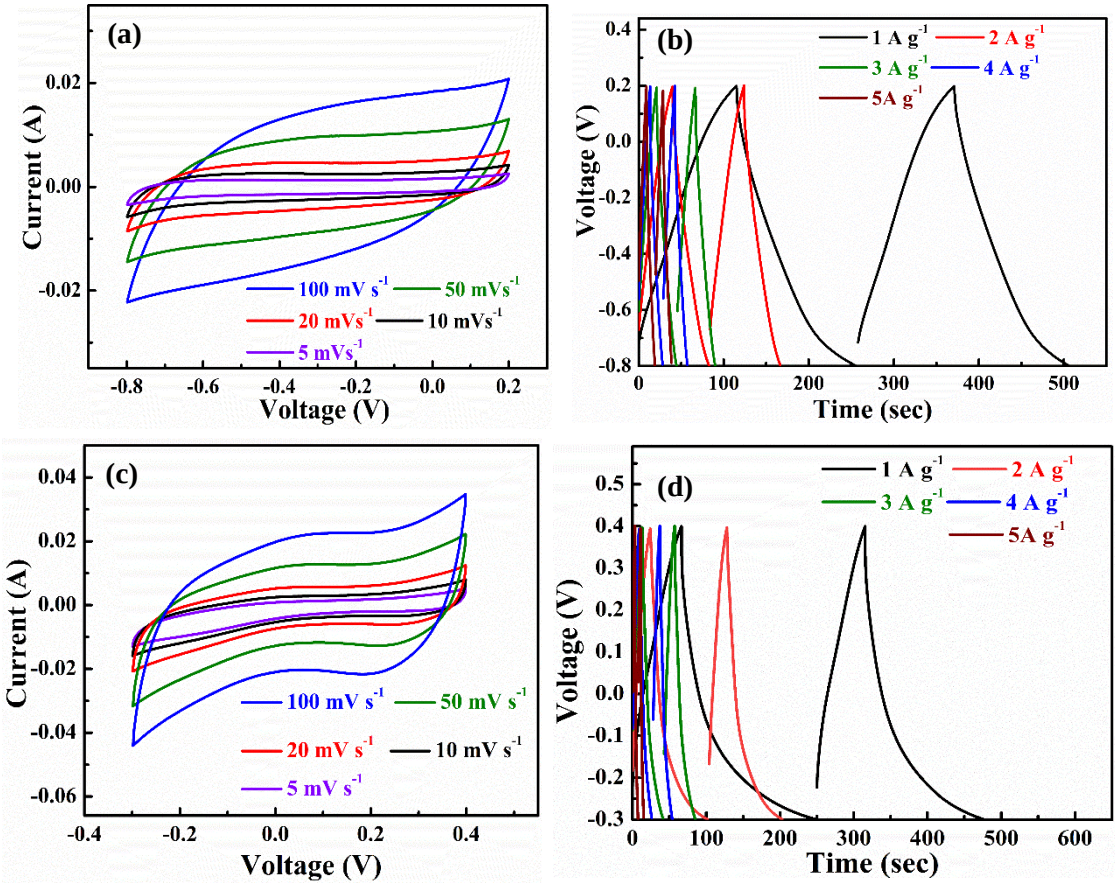

Figure 4.11 *Electrochemical measurements for MoS_2-rGO heterostructure electrode (a) CV curves at different scan rates and (b) GCD curves at different discharge current densities in 1M Na_2SO_4 electrolyte; (c) CV curves at different scan rates, and (d) GCD curves at different discharge current densities in 1M H_2SO_4 electrolyte.*

Figure 4.11 (c) and **4.11 (d)** represents capacitive behaviour of MoS_2-rGO heterostructure electrode in acidic (1M H_2SO_4) electrolyte. The CV curves of **Figure 4.11 (c)** exhibit occurrence of faradic reactions at the electrode/electrolyte interface due to the functional groups of heterostructure along with EDLC. The maximum specific capacitance of 228, 180, 145, 108 and 86 F g^{-1} have been obtained at a sweep rate of 5, 10, 20, 50 and 100 mV s^{-1}. The GCD curves of MoS_2-rGO heterostructure electrodes at different current densities ranging from 1 to 5 A g^{-1} are shown in **Figure 4.11 (d)** for acidic electrolyte, which clearly suggests the deviation from triangular behaviour. The specific capacitance of 230, 222, 120, 97 and 58 F g^{-1} are obtained at discharge current densities of 1, 2, 3, 4 and 5 A g^{-1}, respectively, showing good capacitive sustainability of electrode in acidic electrolyte.

To further understand the kinetics of heterostructure electrode, we have performed EIS study in both aqueous electrolytes. **Figure 4.12 (a)** displays Nyquist plots of MoS_2-rGO heterostructure electrode, fitted using CPE equivalent circuit. The presence of semicircle at higher frequencies and a straight line at the lower frequency region confirms the capacitive behaviour of MoS_2-rGO heterostructure electrode. The lower R_s value for heterostructure electrode in acidic electrolyte is due to the small ionic size of the H^+ ion. The smaller value of R_{CT} for acidic electrolyte (R_{CT} ~ 13.3 Ω) compared to neutral electrolyte (R_{CT}~ 18.7 Ω) suggests fast ion transport in acidic medium at electrode/electrolyte interface. **Figure 4.12 (b)** shows Bode impedance plots indicating nearly equal impedance in both electrolytes. The Bode phase plots of **Figure 4.12 (c)** show the maximum phase angle ~ 61° and 47° in neutral and acidic medium, suggesting pseudocapacitive predominant behaviour for charge storage process in MoS_2-rGO heterostructure electrode in both electrolytes. **Figure 4.12 (d)** shows long term durability of capacitive performance of MoS_2-rGO heterostructure electrodes tested for 2000 cycles at discharge current of 2 A g^{-1} for both neutral and acidic electrolyte. The capacitance

retention of 66% and 85% has been observed for acidic and neutral electrolytes, respectively, after 2000 cycles.

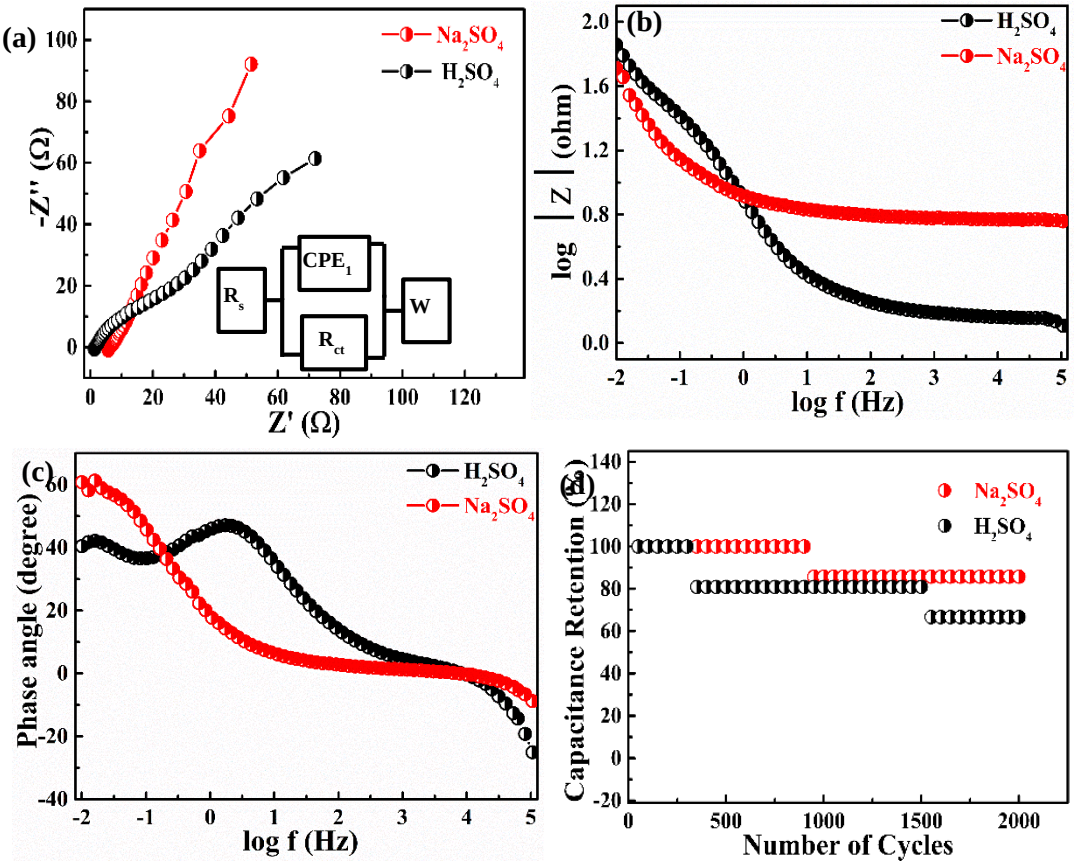

Figure 4.12 *Electrochemical measurements for MoS_2- rGO heterostructure electrode (a) Nyquist plots (inset shows the equivalent circuit), (b) Bode impedance plots, (c) Bode phase angle plots, and (d) Cyclic stability test at a discharge current of 5 A g^{-1} in neutral and acidic electrolytes.*

In summary, the electrochemical study of prepared MoS_2-rGO heterostructure shows higher capacitance in acidic electrolyte compared to neutral one but with lower stability. The present work suggests the improved and sustained capacitive performance of MoS_2-rGO heterostructure in acidic medium is due to the larger dimension and dominance of rGO nanosheets over MoS_2 nanosheets. We have summarized the capacitive performance of rGO, MoS_2 and MoS_2 -rGO based electrodes in **Table 4.1**.

Table 4.1 Capacitive Performance of rGO, MoS_2 and MoS_2 -rGO based Electrodes.

Materials	**Specific Capacitance ($F\ g^{-1}$) in Na_2SO_4**	**Specific Capacitance (Fg^{-1}) in H_2SO_4**	**% Retention /cycles Na_2SO_4**	**% Retention /cycles H_2SO_4**	**Ref.**
rGO-Hydrogel	-	278@ 0.2 Ag^{-1}	-	98/1000	[224]
rGO-KOH treated	-	253@ 0.2 Ag^{-1}	-	102/ 3000	[209]
MoS_2/ Rosette-like	-	137 mF cm^{-2} at 10 mA cm^{-2}	-	81.6/10000	[187]
MoS_2-Mo foil/ Nanosheets	192 @ 1 mA cm^{-2}	-	98/1000	-	[225]
MoS_2/ Sphere-like	106 @ 5 mV s^{-1}	-	93.8/ 1000	-	[226]
MoS_2/ Nanosheets	129.2 @ 1 A g^{-1}	-	85.1 /500	-	[227]
rGO-HH	19 @ 1Ag^{-1}	300@ 1Ag^{-1}	98/1500	95/8000	**Present work**
rGO-Urea	2@ 1Ag^{-1}	220@ 1Ag^{-1}	96/1500	93/8000	**Present work**
2H-MoS_2 nanosheets	173@ 1Ag^{-1}	62@ 1Ag^{-1}	88/2000	70/1500	**Present work**
MoS_2 - nanoflowers	382@ 1Ag^{-1}	68@ 1Ag^{-1}	94/10000	62/2000	**Present work**
MoS_2-rGO heterostructure	136@ 1Ag^{-1}	230@ 1Ag^{-1}	66/2000	85/2000	**Present work**

4.3 Conclusion

In this chapter, we have discussed the optimization of capacitive performance for different rGO and MoS_2 nanostructures and their heterostructure. This study clearly indicated that rGO samples show better capacitive behaviour in acidic electrolyte, while MoS_2 nanostructures show better response in neutral electrolyte. The capacitive behaviour for all prepared samples comprises double layer capacitance and pseudocapacitance both due to the presence of oxygen containing functional groups. The MoS_2-rGO heterostructure shows better capacitive performance in acidic medium compared to neutral one due to the dominance of larger dimension rGO nanosheets in heterostructure. This work identifies the suitable morphologies of rGO and MoS_2 nanostructures for supercapacitor devices with acidic and neutral aqueous electrolytes.